

Recent Advances in Potentiometric Scanning Electrochemical Microscopy

PhD Thesis

author:
András Kiss

supervisor:
prof. Géza Nagy

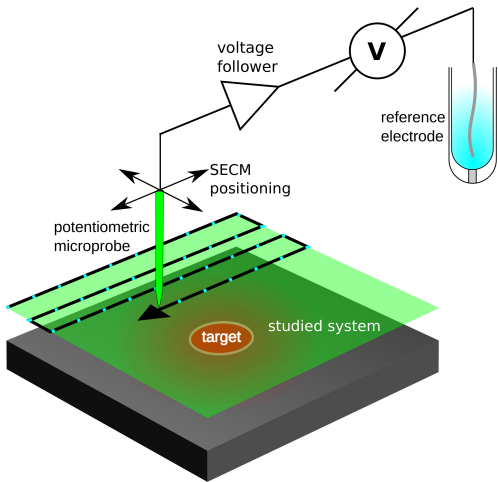
Department of General and Physical Chemistry
University of Pécs, Hungary



April 18, 2017

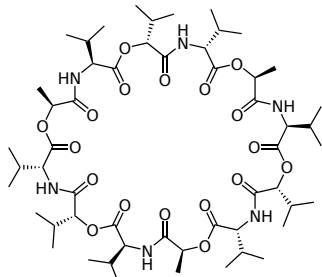
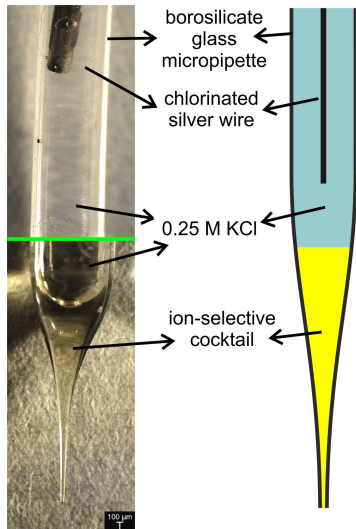
Potentiometric Scanning Electrochemical Microscopy

A Scanning Probe Microscopic technique



Ion-selective micropipettes

As SECM probes



Valinomycin

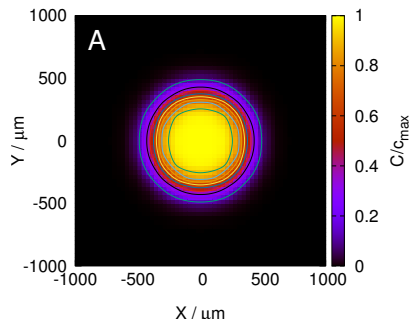
$$E = E^\theta + \frac{RT}{z_i F} \ln \left[a_i + \sum_j \left(k_{ij} a_j^{z_i/z_j} \right) \right]$$

Nikolsky-equation

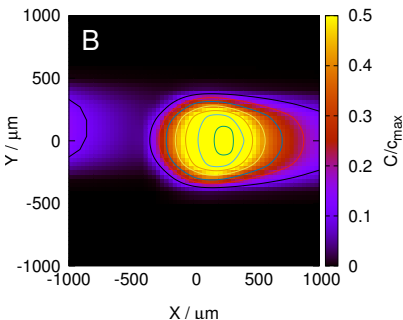
The problem with potentiometric SECM

Distortion at high scan rate

Slow

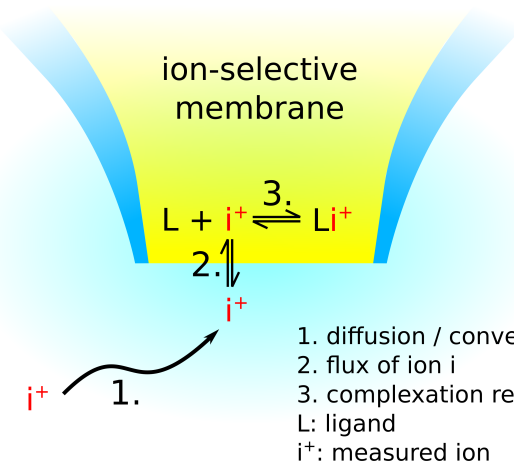


Fast



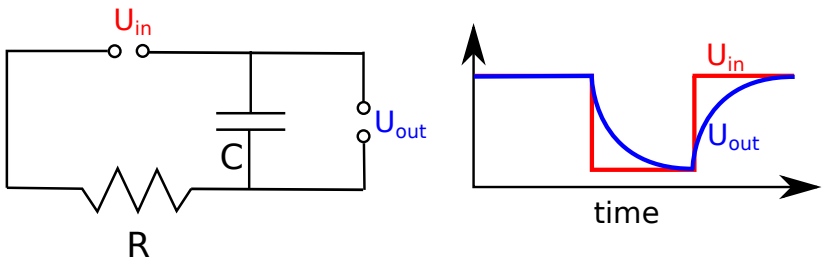
Why is the image distorted?

Possible contributors to the lag



Why is the image distorted?

The RC time constant



The time that is required to charge the capacitor by $\approx 63\%$ ($1 - 1/e$).

$$\tau = R \cdot C$$

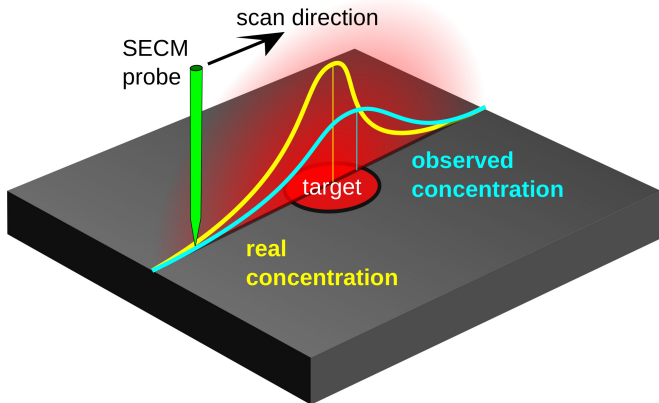
$$R = 5 \text{ G}\Omega$$

$$C = 500 \text{ pF}$$

$$\tau = 2.5 \text{ s}$$

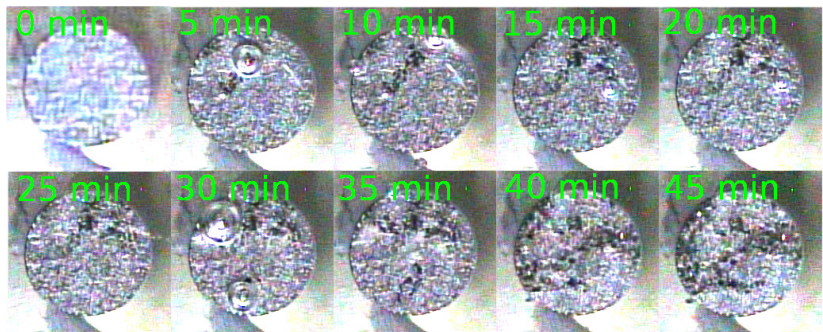
Distortion of potentiometric imaging

In the case of a linescan



Why is it so important to complete the scan quickly?

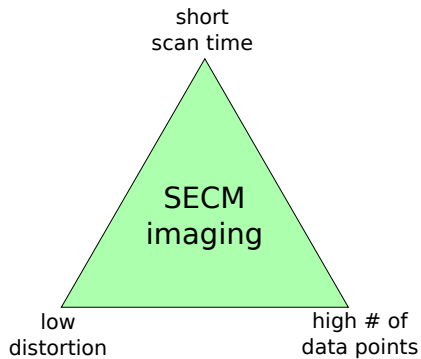
Example: corrosion of a magnesium alloy



Corrosion of the AZ63 magnesium-aluminium-zinc alloy.

Trade-off triangle of potentiometric SECM

Compromise between the three desired competing properties

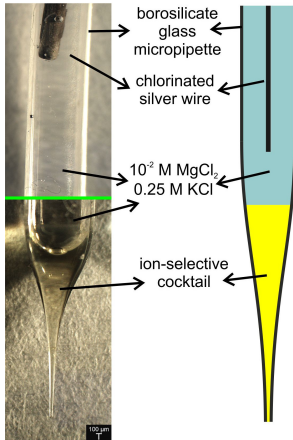


Solution #1: Solid contact micropipettes as SECM probes.

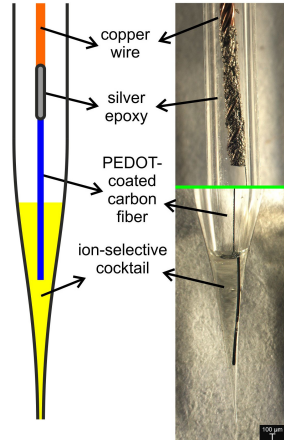
Liquid vs. solid contact micropipettes

Comparison of construction

Liquid contact

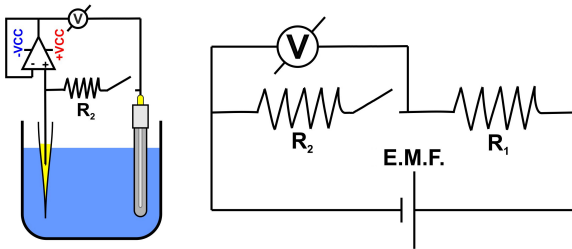


Solid contact



Comparison of the electrodes' resistance

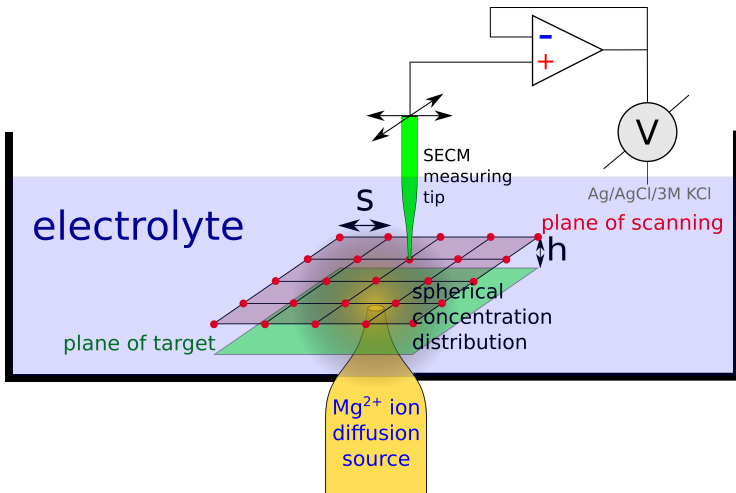
Voltage divider method and result



Type	$R_{ISME} / G\Omega$
Liquid contact	4.80
Solid contact	0.56

Comparison of the electrodes' performance

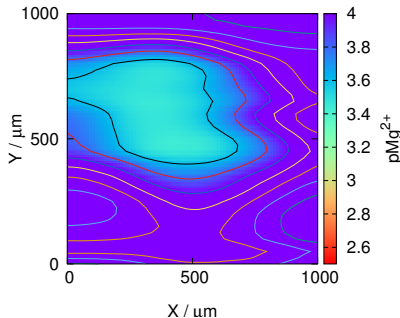
Experimental setup



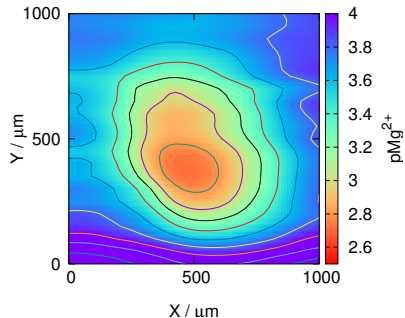
Comparison of the electrodes' performance

Results

Liquid contact

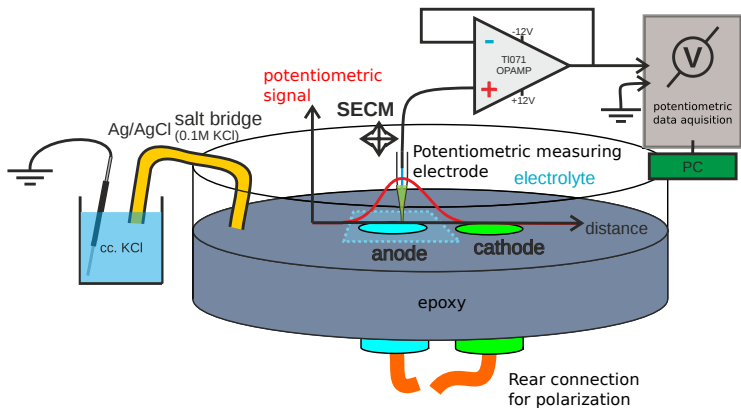


Solid contact



Application in corrosion science: galvanic corrosion of Mg

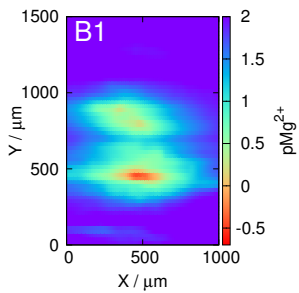
Experimental setup



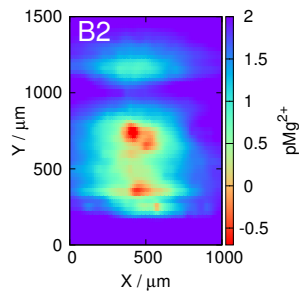
Application in corrosion science: galvanic corrosion of Mg

Results

Liquid contact



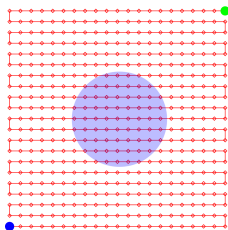
Solid contact



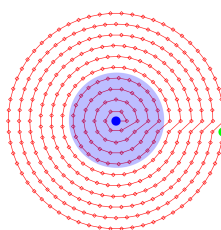
Solution #2: Optimizing scanning patterns and algorithms.

New SECM scanning patterns based on the polar-coordinate system

Cartesian coordinate
system based scanning
pattern



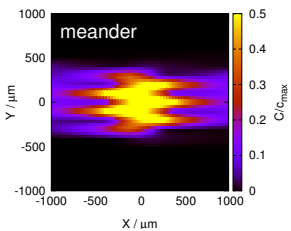
Polar coordinate
system based scanning
pattern



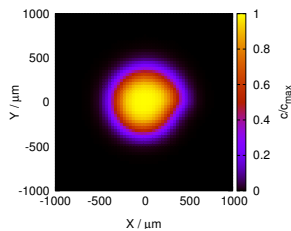
Simulated SECM scans

Using the Cartesian and the polar coordinate system based algorithms

Cartesian



polar



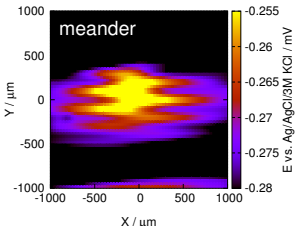
Comparison of the simulated scans

Algorithm	n	time (s)	mean squared error
Meander	441	440	2.75×10^{-2}
Fast comb	441	520	2.07×10^{-2}
Comb	441	881	2.75×10^{-2}
Web	110	109	9.63×10^{-3}
Arc	341	340	2.95×10^{-3}

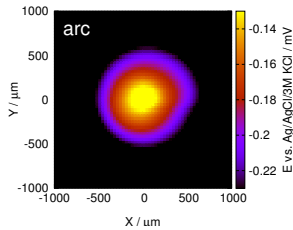
Confirmation with experimental SECM scans

Recorded using the antimony microelectrode

440 seconds



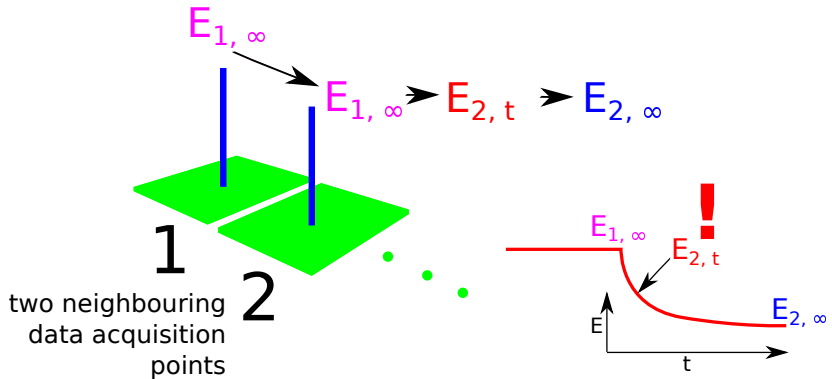
340 seconds



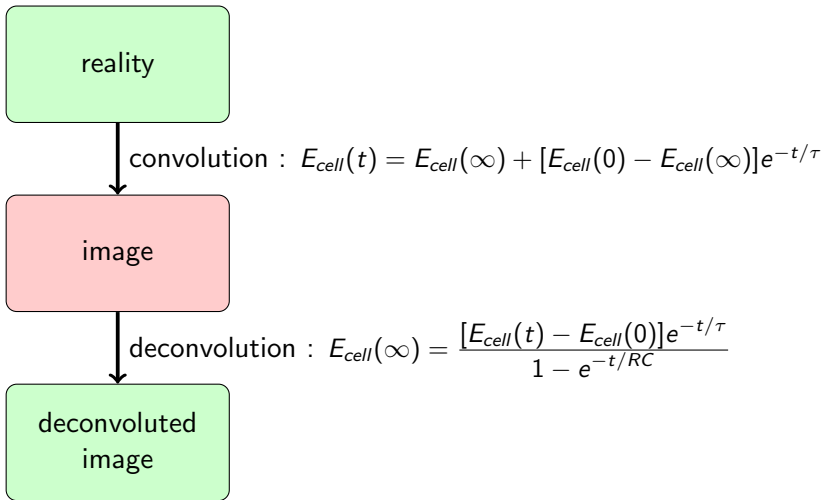
Scans are completed almost 2 times faster,
images have almost 10 times less distortion.

Solution #3: Signal processing.

The convolution function of the distortion

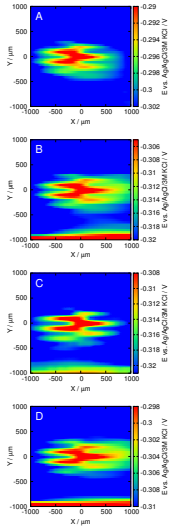


Convolution and deconvolution

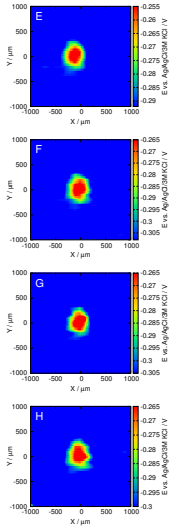


Deconvolution of potentiometric SECM images

Recorded using the antimony microelectrode following the meander algorithm

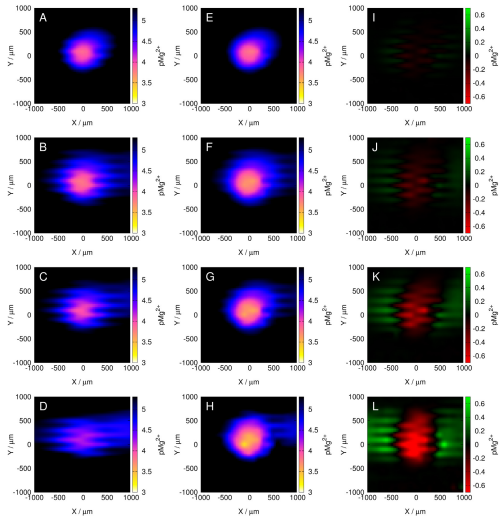


deconvolution
→



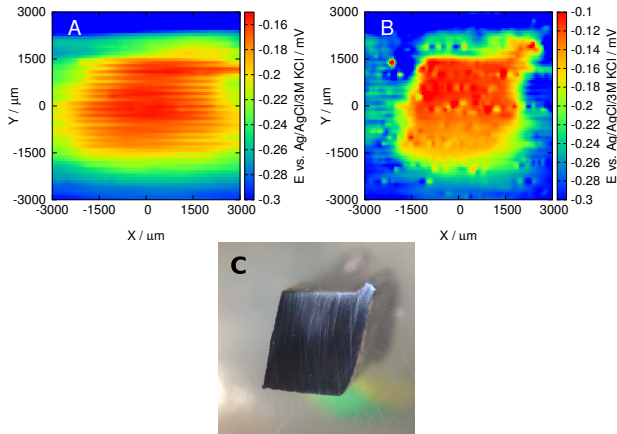
Deconvolution of potentiometric SECM images

Recorded using the magnesium ISME following the meander algorithm



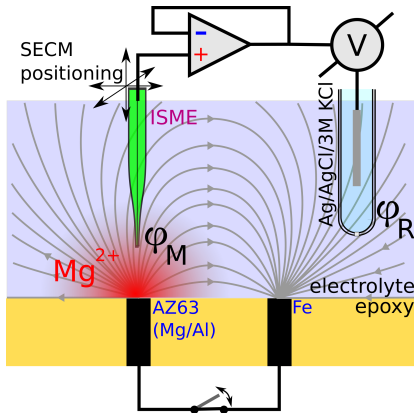
Practical example: corroding carbon steel sample

Scanned with an antimony microelectrode



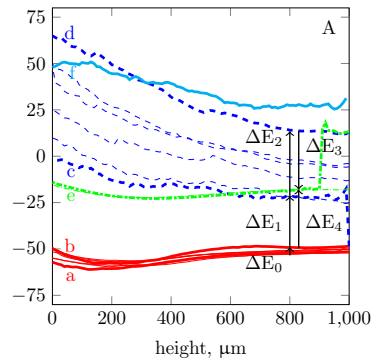
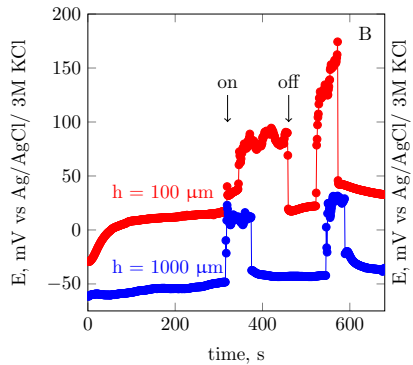
The effect of electric field on potentiometric SECM imaging.

The electric field during galvanic corrosion

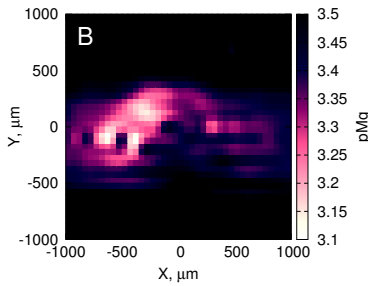
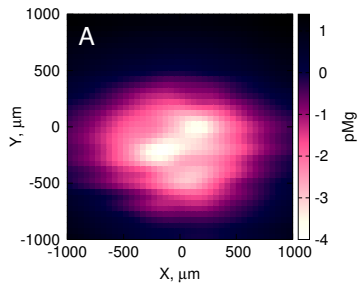


$$\Delta E = E_M - E_R + (\phi_M - \phi_R)$$

The effect of electric field on the measured potential



The effect of electric field on potentiometric SECM imaging



Thesis 1–4

1. I have shown the improved quality of potentiometric SECM images recorded with low resistance, solid-contact magnesium ion-selective microelectrodes. I've compared them to conventional, liquid contact microelectrodes by basic characterization and model system study to prove the improved performance.
2. Taking advantage of the new solid-contact microelectrodes, I have studied the galvanic corrosion of magnesium and the AZ63 magnesium alloy by mapping the concentration of dissolving ions. The new solid contact ion selective microelectrodes allowed faster scan rates.
3. I have estimated the corrosion current based on the SECM measurements, and compared the result with the direct measurement of corrosion current. After applying Faraday's Law of Electrolysis, the two results could be compared. They were very similar, suggesting the applicability of SECM in obtaining quantitative results.
4. I have designed new scanning patterns and algorithms, optimized to radially symmetric targets. I've proven that with these new patterns and algorithms, image distortion is lower compared to the conventional ones, by numerical simulations and experimental SECM scans.

Thesis 5–8

5. I am the first who used deconvolution to reduce distortion in potentiometric SECM images. To prove the validity of the technique, I have compared deconvoluted images to equilibrium images scanned at a rate which allowed to record equilibrium potentials.
6. I have successfully used deconvolution to restore potentiometric SECM images about a corroding carbon steel sample. Evaluation of this data was possible, because scanning time *and* distortion was reduced at the same time.
7. I have shown the possibility of blind deconvolution. This method can be used on measurements where the convolution function cannot be determined.
8. I have successfully resolved the observed discrepancy in recent papers about impossibly high ion activities. The electric field present in many studied systems – galvanically corroding ones in particular – has a direct influence on the measured potential. I have shown how big of an error can it cause. In the system I have studied, the error was almost four orders of magnitude. By taking this effect into account, a more accurate conclusion can be drawn.

List of publications

Related to the dissertation

1. Ricardo M. Souto, **András Kiss**, Javier Izquierdo, Lívia Nagy, István Bitter, Géza Nagy, Spatially-resolved imaging of concentration distributions on corroding magnesium-based materials exposed to aqueous environments by SECM, *Electrochemistry Communications* 26 (2013): 25-28., IF.: 4.85, cited by: 31
2. **András Kiss**, Ricardo M. Souto, Géza Nagy, Investigation of Mg/Al alloy sacrificial anode corrosion with Scanning Electrochemical Microscopy, *Periodica Polytechnica Chemical Engineering* 57, no. 1-2 (2013): 11-14., IF.: 0.30, cited by: 5
3. Javier Izquierdo, **András Kiss**, Juan José Santana, Lívia Nagy, István Bitter, Hugh S. Isaacs, Géza Nagy, Ricardo M. Souto, Development of Mg^{2+} ion-selective microelectrodes for potentiometric scanning electrochemical microscopy monitoring of galvanic corrosion processes, *Journal of The Electrochemical Society* 160, no. 9 (2013): C451-C459., IF.: 3.27, cited by: 23
4. **András Kiss**, Géza Nagy, New SECM scanning algorithms for improved potentiometric imaging of circularly symmetric targets, *Electrochimica Acta* 119 (2014): 169-174., IF.: 4.50, cited by: 8
5. **András Kiss**, Géza Nagy, Deconvolution of potentiometric SECM images recorded with high scan rate, *Electrochimica Acta* 163 (2015): 303-309., IF.: 4.50, cited by: 7
6. **András Kiss**, Géza Nagy, Deconvolution in potentiometric SECM, *Electroanalysis* 27, no. 3 (2015): 587-590., IF.: 2.14, cited by: 2
7. **András Kiss**, Dániel Filotás, Ricardo M Souto, Géza Nagy, The effect of electric field on potentiometric Scanning Electrochemical Microscopic imaging, *Electrochemistry Communications* 77 (2017): 138-141., IF.: 4.569

List of publications

Unrelated to the dissertation

8. András Kiss, László Kiss, Barna Kovács, Géza Nagy, Air Gap Microcell for Scanning Electrochemical Microscopic Imaging of Carbon Dioxide Output. Model Calculation and Gas Phase SECM Measurements for Estimation of Carbon Dioxide Producing Activity of Microbial Sources, *Electroanalysis 23, no. 10* (2011): 2320-2326., IF.: 2.14, cited by: 3
9. Ricardo M. Souto, Javier Izquierdo, Juan José Santana, András Kiss, Lívia Nagy, Géza Nagy. Progress in scanning electrochemical microscopy by coupling potentiometric and amperometric measurement modes, *Current Microscopy Contributions to Advances in Science and Technology, Formatec Research Center, Badajoz* (2012): 1407-1415, cited by: 3
10. Lívia Nagy, Gergely Gyetvai, András Kiss, Ricardo Souto, Javier Izquierdo, Géza Nagy, Speciális célra szolgáló mikroelektródok kifejlesztése és alkalmazása, *Magyar Kémiai Folyóirat 119, 2-3.* (2013): 104-109.
11. Zsuzsanna Őri, András Kiss, Anton Alexandru Ciucu, Constantin Mihailciuc, Cristian Dragos Stefanescu, Lívia Nagy, Géza Nagy, Sensitivity enhancement of a „bananatrode” biosensor for dopamine based on SECM studies inside its reaction layer, *Sensors and Actuators B: Chemical 190* (2014): 149-156., IF.: 4.10, cited by: 4
12. Javier Izquierdo, Bibiana M Fernández-Pérez, Dániel Filotás, Zsuzsanna Őri, András Kiss, Romen T Martín-Gómez, Lívia Nagy, Géza Nagy, Ricardo M Souto, Imaging of Concentration Distributions and Hydrogen Evolution on Corroding Magnesium Exposed to Aqueous Environments Using Scanning Electrochemical Microscopy, *Electroanalysis 28*, (2016): 2354-2366., IF.: 2.471, cited by: 2
13. A. El Jaouhari, Dániel Filotás, András Kiss, M. Laabd, E. A. Bazaaroui, Lívia Nagy, Géza Nagy, A. Albourine, J. I. Martins, R. Wang, SECM investigation of electrochemically synthesized polypyrrole from aqueous medium, *Journal of Applied Electrochemistry 46* (2016): 1199-1209., IF.: 2.223

Acknowledgements

I wish to express my sincere gratitude to **professor Dr. Géza Nagy** for introducing me to the fascinating field of electrochemistry, and for the continuous support and guidance during the work.

I am truly grateful to **Dr. Barna Kovács** for the enlightening discussions about microelectrode electronics. and to **Dr. Lívia Nagy** for the help received during the years of my PhD studies. I am also thankful to **Dr. Sándor Kunsági-Máté** for the support.

I am thankful to **Dr. Lajos Höfler** and **Dr. Balázs Csóka** for reviewing my dissertation draft. I am also thankful to all the anonymous referees who gave meaningful feedback about my work as part of the peer review process.

I am thankful to Professor Johan Bobacka, Ricardo M. Souto, Frank-Michael Matysik, Petr Skládal and Mohammed Bazzaoui for welcoming me in their laboratories.

Many thanks are due to all my colleagues and friends with whom I have worked during my years as an undergraduate and doctoral student.

Thank you for your attention.

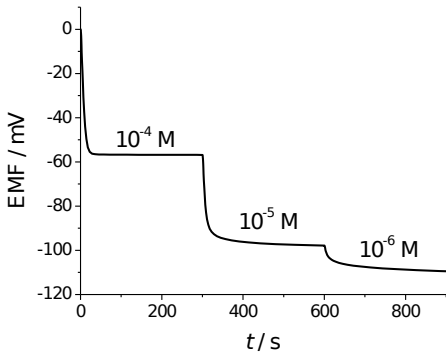
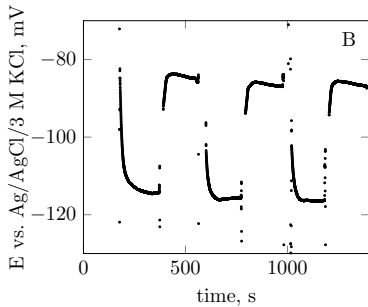
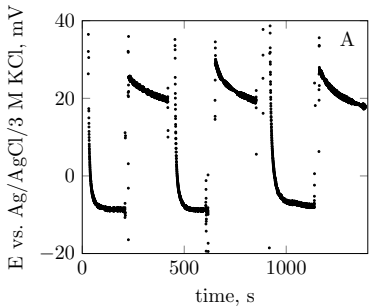
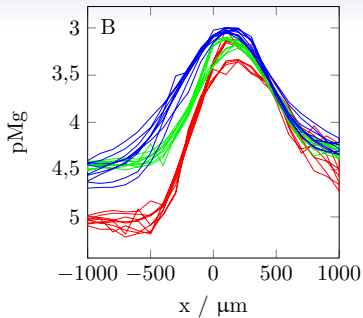
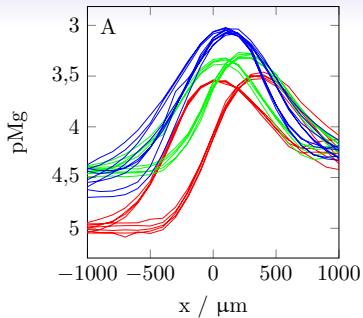


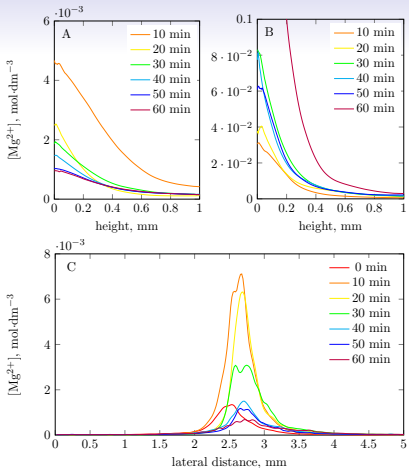
Figure 1. Nernst-Planck-Poisson simulation of the response of a potentiometric ion-selective sensor to decreasing primary ion activities. Relatively large activity of interfering ions is maintained ($a_J = 1\text{mM}$) to keep the whole cell R constant. Adhered layer thickness $100 \mu\text{m}$, $K_{IJ} = 10^{-3}$.



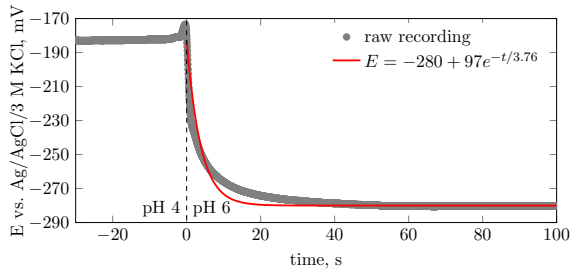
Dynamic response curves obtained for response time measurements to changes in $MgCl_2$ concentrations of 10^{-1} M and 10^{-2} M, in 10^{-3} M NaCl. (A) liquid-contact, and (B) solid-contact Mg^{2+} ISME.



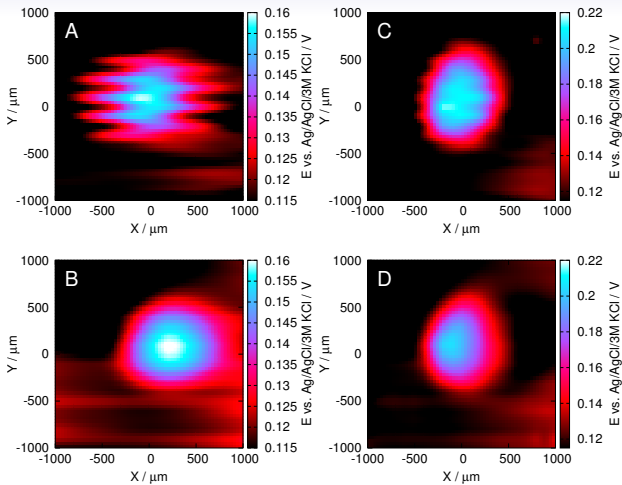
(A) Raw scan lines recorded $h = 100 \mu\text{m}$ over the center of the pipette orifice, which served as a Mg^{2+} ion diffusion source. (B) Scan lines obtained after deconvolution. t_e equilibration intervals were 4.9 s (blue), 1.9 s (green), and 0.4 s (red). Probe movement speed was $1000 \mu\text{m}/\text{s}$, and probe movement interval was 0.1 s. 8 scan lines were recorded in each case, 4 forward, 4 reverse scans.



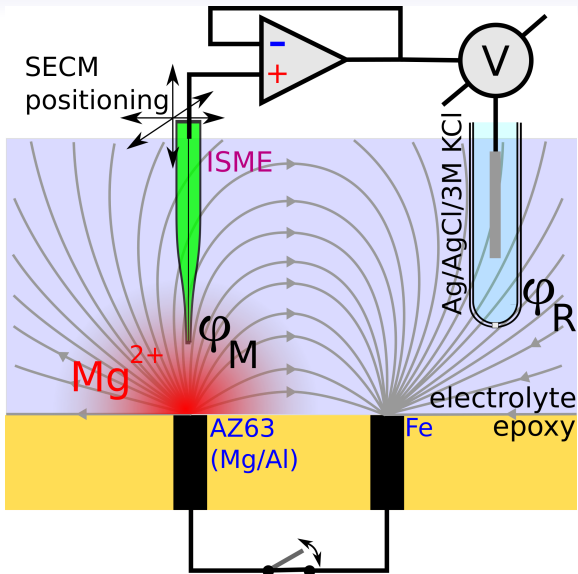
(A, B) Retracting and (C) lateral SECM linescans above the AZ63 magnesium-aluminium-zinc alloy sample initiated at different instances in time. The AZ63 sample first was corroding spontaneously (A), then galvanically coupled to the iron sample (B). Lateral scans in (C) were recorded above the uncoupled AZ63 sample. Scan rate: 10 $\mu\text{m}/\text{s}$.

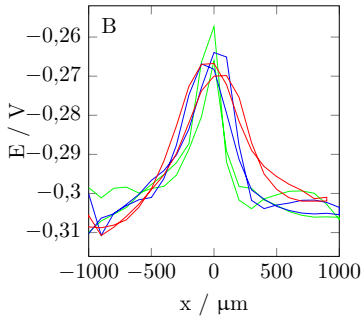
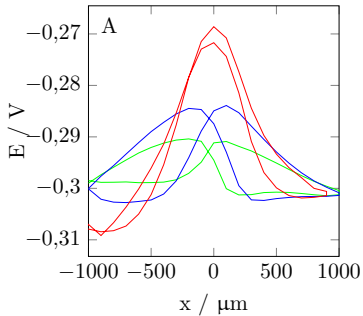


Transient response of the antimony microelectrode to analyte activity step. The measuring and reference electrodes were dipped into buffer solutions with $\text{pH} = 4$ before the measurements started, and $\text{pH} = 6$ at $t = 0 \text{ s}$, respectively. Eq. 4.2 was fitted (red line) on the measurement (gray marks) from the pH step to the end of the curve when potential reaches equilibrium in the $\text{pH} = 6$ buffer.



SECM images before (A-B) and after (C-D) deconvolution. Images recorded with the (A) meander algorithm and (B) fast comb algorithm. Scans conducted with solid contact K^+ ion-selective micropipette.





(A) Raw, and, (B) deconvoluted SECM linescans above the center of the target, at $h = 100 \mu\text{m}$ height, using three different equilibration periods: 0.5 s, (green), 1 s, (blue), and 5 s, (red).